

Doppler Tomography of Relativistic Accretion Disks

Vladimír KARAS* and Pavel KRAUS

*Astronomical Institute, Charles University, Švédská 8,
CZ-150 00 Prague, Czech Republic*

Scheduled for
Publications of the Astronomical Society of Japan,
Vol. 48 (October 1996)

*Also at Scuola Internazionale Superiore di Studi Avanzati, Trieste; Department of Astronomy and Astrophysics, Göteborg University and Chalmers University of Technology, Göteborg

Abstract

Spectral lines from a source orbiting around a compact object are studied. Time variations of observed frequency and count rate due to motion of the source and gravitational lensing are considered. Gravitational field of the central object is described by the Kerr metric. It is shown that: (i) simultaneous temporal and frequency resolution enables us to restrict parameters of the model (inclination angle, position of the source, angular momentum of the black hole); (ii) techniques of image restoration, familiar from other fields of astronomy, can be applied to study inner regions of active galactic nuclei. This contribution is relevant for extremely variable X-ray sources with high parameter of efficiency, such as Seyfert 1 galaxy PHL 1092 observed by *ROSAT*.

Key words: Galaxies: active — Accretion, accretion discs — X-rays: galaxies — Black hole physics

1. Introduction

Tomography is a method of image restoration which has been successfully applied in various fields, particularly in medicine. Image reconstruction, on the other hand, is one of the typical problems in astronomy where the situation is rather specific because astronomical objects are very distant and can be viewed from a single direction only. Rotation of the source is thus essential, and one needs to understand how rotational motion is linked to observed profiles of spectral lines. Vogt, Penrod & Hatzes (1987) describe the tomographical method for mapping the surface of rotating stars. It is assumed that irregularities (spots) on the stellar surface radiate in a spectral line, observed frequency of which is periodically affected by the Doppler effect. An analogous approach was applied in order to study accretion disks in cataclysmic variable stars (Marsh, Horne 1988; Kaitchuck et al. 1994) and Algol-type binaries (Albright, Richards 1996). It has been demonstrated that Doppler tomography can be very useful for tracing the structure of the disk surface when it is seen at a sufficiently large inclination. Similar techniques have been used recently to study detached binaries and multiple stars (Simon, Sturm 1994; Hadrava 1995). All these methods are based on the fact that the line spectrum of the source is affected by the radial velocity of its

individual components with respect to the observer. Knowing the composite spectrum at different phases, the problem of the line formation can be inverted and contributions from separate components of the source can be revealed.

The present paper deals with two topics: (i) the applicability of Doppler tomography to study rotation and surface structure of disks around compact objects is discussed, and (ii) the relevance of time-resolved spectral-line profiles for study of the rapid X-ray variability of active galactic nuclei (AGN) is explored. (As for Doppler tomography, we retain the original terminology, although it is less appropriate in the context of general relativity in which the distinction between Doppler shift and the gravitational shift of the photon energy cannot be defined unambiguously.) The motivation for investigating these problems comes from a widely accepted model of AGNs with a central black hole surrounded by an accretion disk (see, e.g., Rees 1984). It has been realized by several authors that double-peaked asymmetric profiles of the H α line observed in some galactic nuclei can be explained by relativistic effects (Chen, Halpern, Filippenko 1989; Eracleous, Halpern 1994). Theoretical line profiles have been studied by numerous authors who also discussed specific effects of general relativity: frame dragging (Kojima 1991; Laor 1991; Bromley, Chen, Miller 1996), multiple images (Bao, Hadra, Østgaard 1994), and self-gravity of relativistic disks (Karas, Lanza, Vokrouhlický 1995).

For a long time, some AGNs have been recognized as rapidly variable X-ray sources (Feigelson et al. 1986; Mushotzky, Done, Pounds 1993; Papadakis, Lawrence 1995). Apart from blazars, the class of I Zw 1 objects (Phillips 1976; Boller et al. 1993) has been distinguished by the high value of their efficiency parameter: $\eta \approx 5 \times 10^{-43} \Delta L_X / \Delta t \gtrsim 0.1$ (Fabian 1979). This parameter characterizes temporal change of the source X-ray luminosity, ΔL_X [erg s $^{-1}$], during the relevant variability time-scale $\Delta t \approx 10^2$ – 10^5 seconds. For example, a member of the I Zw 1 class, narrow-line Seyfert 1 galaxy PHL 1092 has recently been studied in detail (Forster, Halpern 1996) and it has been speculated that the remarkably high value of its efficiency parameter ($\eta \gtrsim 0.6$) calls for a non-standard model of the object (strongly anisotropic emission or accretion onto an extremely rotating black hole; Kwan et al. 1995). It is suggested in the present contribution that the lensing effect acting on a source of radiation orbiting a black hole (as discussed by numerous authors in another context; cf. Abramowicz, Bao, Lanza, Zhang 1991;

Rauch, Blandford 1994) should also be considered as a possible explanation of such extreme variability. The model can be submitted to an observational test by studying time-resolved spectral lines which are formed in that region of the source responsible for variability. Observations have not yet provided sufficient resolution for serious spectroscopy of this type.

The most prominent relativistic effects can be expected for spectral features around 7 keV because this complex is presumably formed in the innermost regions of accretion disks (Fabian, George 1991; Matt, Perola, Piro, Stella 1992). The improved technology of *ASCA*'s detectors makes high-resolution spectroscopy of the X-ray sources feasible (Serlemitsos et al. 1995) so that the above-mentioned theoretical works on line profiles now become timely. Possible future X-ray spectroscopy missions will provide temporal resolution of the spectral lines which has not yet been much discussed in the literature. The subsequent section of this paper deals with predicted line profiles as a function of time. Specific features of the frequency shift relevant for the tomographical method of the disk mapping are mentioned. The main aim of this discussion is to point out the differences between accretion disks around compact objects and other situations where the effects of relativity are negligible.

2. Doppler Tomography of Accretion Disks

2.1 *Details of the Model*

It is assumed that a localized region of enhanced emissivity is located on the surface of an accretion disk. The possible existence of such irregularities has been discussed by several authors because it has important consequences for variability of AGNs (Abramowicz, Lanza, Spiegel, Szuszkiewicz 1992; Sivron, Caditz, Tsuruta 1996). It is assumed that the disk resides in the equatorial plane of a Kerr black hole. It will be shown that the observed flux and frequency of a spectral line as functions of time determine, to a certain degree, the inclination of the disk and the angular-momentum parameter of the black hole, a ($0 \leq a \leq 1$). The relative frequency shift g of radiation (ratio of frequency observed by a distant observer to frequency emitted in a

local frame corotating with the disk material) can be expressed, within the approximation of geometrical optics, in terms of four-momentum of photons, \mathbf{p} , and four-velocities \mathbf{u}_{em} , \mathbf{u}_{obs} of the emitting material and of the distant observer, respectively:

$$g \equiv \frac{\nu_{\text{obs}}}{\nu_{\text{em}}} = \frac{\mathbf{p} \cdot \mathbf{u}_{\text{obs}}}{\mathbf{p} \cdot \mathbf{u}_{\text{em}}}; \quad (1)$$

g is a function of polar coordinates $\{r, \phi\}$ in the disk plane, defined in such a way that $\{\phi = 0, \theta = \theta_{\text{obs}}\}$ represents a direction to the observer ($\theta_{\text{obs}} = 90^\circ$ when the disk is seen edge-on). In order to minimize the number of free parameters, Keplerian rotation law is assumed: $\Omega \propto 1/(r^{3/2} + a)$ in usual dimensionless geometrized units. This restriction is in agreement with our assumption of geometrically thin, equatorial disk. The method can be applied to a different rotation law analogously.

Radiation flux from the source is obtained by integrating the observed intensity I_{obs} over the observer's local sky. The resulting value of the flux is determined by distribution of g and I_{em} (locally emitted intensity) in the disk ($I_{\text{obs}}/I_{\text{em}} = g^3$), and it also depends on the shape of light trajectories which are affected by the presence of the central object (lensing effect). Various semi-analytical and completely numerical approaches have been developed for efficient integration of the observed radiation flux (Pineault, Roeder 1977; Luminet 1979; Asaoka 1989). We employed the method described by Karas, Vokrouhlický & Polnarev (1992).

2.2 Line Profiles Resolved in Time

First, it is instructive to approximate light rays by straight lines because the problem of observed line profiles can then be solved analytically without difficulty (Gerbal, Pelat 1981; Kojima 1991). Let us consider a point-like source moving along a circular orbit with radius $r = r_{\text{em}}$ and emitting, in its rest frame, a spectral line with Dirac function-type profile:

$$I_{\text{em}}(\nu, r, \phi) \propto \delta(\nu - \nu_{\text{em}})\delta(r - r_{\text{em}})\delta(\phi - \Omega t). \quad (2)$$

The observed flux from a single source is a simple periodic function of time,

$$F(\nu, t) \propto \int g^3 I_{\text{em}}(\nu/g, r, \phi - r \cos \phi \sin \theta_{\text{obs}}), \quad (3)$$

and its observed phase φ can thus be normalized to the unit interval, $0 \leq \varphi \leq 1$. The constant of proportionality in eq. (3) is undetermined unless a specific physical mechanism generating radiation is assumed, but for the ratio of the count rates at the maximum and the minimum observed frequency one can write

$$\frac{F(\nu_{\max})}{F(\nu_{\min})} = \frac{\nu_{\max}^3}{\nu_{\min}^3}, \quad \frac{\nu_{\max}}{\nu_{\min}} = \frac{r_{\text{em}}^{1/2} + \sin \theta_{\text{obs}}}{r_{\text{em}}^{1/2} - \sin \theta_{\text{obs}}}; \quad (4)$$

r_{em} can be estimated from relation (4). Superposition of radiation from multiple sources results in a fluctuating signal but, in principle, individual contributions can still be restored. In practice, however, temporal and frequency resolution of observational data is limited, and one has to work with a more complicated local profile of the line. An appropriate technique of image restoration has been discussed by Marsh & Horne (1988). These authors ignored any relativistic corrections (frequency shift was determined solely by radial velocity of the source), nevertheless, their approach can be applied to our situation if eqs. (1)–(2) for the redshift factor and intensity are taken into account. The difference becomes evident upon comparison of our Fig. 1 with Fig. 1 of Marsh & Horne: Notice the asymmetry of isocontours of g with respect to the vertical axis. The shape of the contour-lines is determined by mutual competition of the overall gravitational redshift with the Doppler effect due to rotation (right-hand side of the disk approaches the observer and the corresponding observed frequency is thus increased). As a result of this asymmetry, observed profiles of spectral lines are also asymmetric about the emitted frequency.

The lensing effect, neglected in the discussion above, calls for a correction of the observed flux. The magnitude of the error introduced by this neglect was discussed by several authors (Kojima [1991] corrects an inconsistency in the work of Gerbal & Pelat [1981], but, in most situations, the difference does not produce a visible change in line profiles). Apparently, the correction becomes important when most of the radiation is generated near a black-hole horizon (typically, $r \lesssim 20 r_g$, $r_g \equiv 1 + \sqrt{1 - a^2}$) or when observer inclination is large ($\theta_{\text{obs}} \gtrsim 75^\circ$). The approximation of straight photon trajectories is unable to reflect lensing effects and we thus turn to a more sophisticated treatment by solving the geodesic equation in the Kerr metric.

Fig. 2 illustrates variations of the line profile of a source in the Keplerian circular motion around a Schwarzschild black hole ($a = 0$). It is assumed

that the source has the form of a spot radiating isotropically in its local frame. Local emissivity has a Gaussian frequency profile ($\text{FWHM} \approx 0.2$). Local intensity decreases exponentially with the distance from the centre of the spot. The characteristic diameter d of the spot is defined by requiring that intensity at the edge of the spot decreases by a factor $1/e$ in comparison with the value in the centre. In our example, $d \approx 1 r_g$. The resulting observed profile is not sensitive to the assumptions above, provided

$$2\pi r_{\text{em}} \gg d, \quad \text{FWHM} \ll \frac{\nu_{\text{max}} - \nu_{\text{min}}}{\nu_{\text{max}} + \nu_{\text{min}}}. \quad (5)$$

The local profile of the line is centred around ν_{em} but the observed profile oscillates around a lower value of frequency (observed centroid frequency) because of the gravitational redshift. The maximum frequency corresponds to the source approaching the observer ($\varphi \approx \frac{3}{2}\pi$), the minimum frequency corresponds to the source receding from the observer ($\varphi \approx \frac{1}{2}\pi$). The observed count rate follows this variation strictly only if lensing and time delay are ignored (cf. eq. [3]). On the other hand, once these effect are take into account properly, the count rate has its maximum somewhere within the interval $\pi \lesssim \varphi \lesssim \frac{3}{2}\pi$, depending on θ_{obs} . Two well-separated local maxima of the count rate can be found in the signal. Lensing effect is responsible for enhancement at $\varphi \approx 0.5$ but the corresponding peak is visible only if $\theta_{\text{obs}} \gtrsim 75^\circ$ (Fig. 2a). Doppler shift produces a peak at $\varphi \approx 0.7$. One can estimate inclination by fitting the line profiles resolved in frequency and time, while with frequency integrated light curves such an estimate is rather uncertain (it can be shown that the phase of the maximum of frequency integrated signal depends only weakly on a and θ_{obs} ; cf. Fig. 8 of Karas, Vokrouhlick & Polnarev 1992). Since the geodesic equation was solved for each of the rays, the correct relation between the orbital phase ϕ of the source on the disk surface and the the phase φ of the observed signal is automatically taken into account. In the case of a rotating black hole, line profiles take a similar course but the frequency range and phase of the maximum are different, as illustrated in the next figure.

A relation between the observed frequency and the count rate is further explored in Fig. 3 where the centroid frequency of the line is given in terms of the count rate. The variable part of the count rate is normalized to unit interval. The centroid frequency is normalized to the local centroid frequency of the line profile in the frame comoving with the source. It is worth noticing

that the maximum and the minimum centroid energy ($\nu_{c,\max}$, $\nu_{c,\min}$) and the observed frequency of the maximum count rate ($\bar{\nu}$) are specific indicators which relate each of the curves to the corresponding values of θ_{em} , r_{em} , and a (Table 1). One can define the relative difference of the centroid frequencies:

$$\Delta\nu_c \equiv \frac{\nu_{c,\max}}{\nu_{c,\min}} - 1 \quad (6)$$

which increases with θ_{obs} increasing and r_{em} decreasing. Large values of $\Delta\nu_c$ ($\gtrsim 0.5$) correspond to relativistic motion of the orbiting source, while small $\bar{\nu}$ ($< \nu_{c,\max}$) indicate the focussing effect to be important. One can verify from Tab. 1 that, for large inclination, $\bar{\nu}$ decreases with r_{em} increasing, while for small inclination the dependence is reversed. Parameters $\Delta\nu_c$ and $\bar{\nu}$ supplement the asymmetry parameter \mathcal{A} which was introduced by Gerbal & Pelat (1981, eq. [13]) in order to characterize asymmetry of the time-integrated line profiles.

3. Conclusion

The sufficient resolution, both in time and frequency, is crucial for practical applicability of Doppler tomography and this is presently the main difficulty of the method in studying inner regions of accretion disks in AGNs. In the present contribution we concentrated on properties of radiation from a single orbiting source, taking into account gravitational lensing of a Kerr black hole. This is the point where the situation differs from previous works—otherwise the techniques of image restoration can be applied in a similar manner as has been done for tracing, e.g., stellar surfaces or detached binary systems.

Orbital motion of the source around a black hole results in variations of the observed count rate and increases the efficiency parameter of the source. This may be a relevant explanation for some extremely variable X-ray objects from the I Zw 1 class, and its relevance can be tested by studying line profiles in time. The method restricts possible values of inclination angle of the disk and angular momentum of the black hole, and it should thus be taken into account in planning future X-ray observations.

We assumed that the source of light radiates isotropically in its local comoving frame, and that it rotates in accordance with the Kepler law. The assumption about local emissivity does not play a particular role in our discussion of the line profiles (Fig. 1) because we did not consider general relativistic bending of light trajectories. Fully relativistic treatment of Figs. 2–3 is however affected by this constrain. Also the rotation law needs to be determined in accordance with the physical situation (equatorial motion around a Kerr black hole, in our case). Otherwise, it introduces another free parameter which must be determined by systematic exploration of the parameter space and fitting values from Tab. 1 to actual data.

This work has been supported by the grants GACR 205/94/0504 and GACR 202/96/0206 in Czech Republic, and by Wenner-Gren Center Foundation in Sweden.

References

Abramowicz M. A., Bao G., Lanza A., Zhang X.-H. 1991, A&A 245, 454

Abramowicz M. A., Lanza A., Spiegel E. A., Szuszkiewicz E. 1992, Nature 356, 41

Albright G. E., Richards M. T. 1996, ApJ 459, L99

Asaoka I. 1989, PASJ 41, 763

Bao G., Hadrava P., Østgaard E. 1994, ApJ 435, 55

Boller Th., Trümper J., Molendi S., Fink H. et al. 1993, A&A 279, 53

Bromley B. C., Chen K., Miller W. A. 1996, ApJ, submitted

Eracleous M., Halpern J. P. 1994, ApJSS 90, 1

Chen K., Halpern J. P., Filippenko A. V. 1989, ApJ 339, 742

Fabian A. 1979, Proc. Roy. Soc. London, Ser. A 366, 449

Fabian A. C., George I. M. 1991, in Iron-Line Diagnostics in X-Ray Sources, eds A. Treves, G. C. Perola, L. Stella (Springer-Verlag, Berlin), p. 169

Feigelson E. D., Bradt H., McClintock J., Remillard R. et al. 1986, ApJ 302, 337

Forster K., Halpern J. P. 1996, ApJ, to appear

Gerbal D., Pelat D. 1981, A&A 95, 18

Hadrava P. 1995, A&AS 114, 393

Kaitchuck R. H., Schlegel E. M., Honeycutt R. K., Horne K. et al. 1994, ApJSS 93, 519

Karas V., Lanza A., Vokrouhlický D. 1995, ApJ 440, 108

Karas V., Vokrouhlický D., Polnarev A. 1992, MNRAS 259, 569

Kojima Y. 1991, MNRAS 250, 629

Kwan J., Chen F.-Z., Fang L.-Z., Zheng W., Ge J. 1995, ApJ 440, 628

Laor A. 1991, ApJ 376, 90

Luminet J.-P. 1979, A&A 75, 228

Marsh T. R., Horne K. 1988, MNRAS 235, 269

Matt G., Perola G. C., Piro L., Stella L. 1992, A&A 257, 63

Mushotzky R. F., Done C., Pounds K. A. 1993, ARA&A 31, 717

Papadakis I. E., Lawrence A. 1995, MNRAS 272, 161

Phillips M. M. 1976, ApJ 208, 37

Pineault S., Roeder R. C. 1977, ApJ 213, 548

Rauch K. P., Blandford R. D. 1994, ApJ 421, 46

Rees M. J. 1984, ARA&A 22, 471
Serlemitsos P. J., Jalota L., Soong Y., Kunieda H. et al. 1995, PASJ 47, 105
Simon K. P., Sturm E. 1994, A&A 281, 286
Sivron R., Caditz D., Tsuruta S. 1996, ApJ, in press
Vogt S. S., Penrod G. D., Hatzes A. P. 1987, ApJ 321, 496

Figure Captions

Fig. 1. Lower panels: Lines of equal frequency shift g on an equatorial accretion disk in Keplerian rotation around a Schwarzschild black hole. Observer looks from the bottom of the page ($\phi = 0$). Both graphs are drawn with radial coordinate $x \equiv 1 - 3r_g/r$ ($r_g = 2$, $0 \leq x \leq 1$). The whole equatorial plane outside the inner edge of the disk is thus captured in this illustration; dotted circles corresponds to $x = 1$. Observer inclination is (a) 80° and (b) 20° . Upper panels: Observed count rates (eq. [3]) from a point-like source orbiting at $r_{\text{em}} = 3r_g$ (solid line) and $r_{\text{em}} = 8r_g$ (dashed line). The count rate is in arbitrary units; frequency is normalized to ν_{em} .

Fig. 2. Time variation of the line profile from a source near a Schwarzschild black hole; (a) $r_{\text{em}} = 14r_g$, $\theta_{\text{obs}} = 80^\circ$; (b) $r_{\text{em}} = 14r_g$, $\theta_{\text{obs}} = 20^\circ$; (c) $r_{\text{em}} = 4r_g$, $\theta_{\text{obs}} = 20^\circ$. Count rate is normalized to the maximum value; frequency is normalized to ν_{em} . The phase interval corresponding to one revolution of the source is shown ($0 \leq \varphi \leq 1$). See the text for details.

Fig. 3. Centroid frequency versus count rate. Each loop characterizes one complete revolution of the source at given r_{em} . Three different radii of the orbit have been chosen, as indicated by the line-style: $r_{\text{em}} = 3r_g$ (solid line); $r_{\text{em}} = 5r_g$ (dashed line); $r_{\text{em}} = 8r_g$ (dot-dashed line). Four panels are shown: (a) $\theta_{\text{obs}} = 80^\circ$, $a = 0$; (b) $\theta_{\text{obs}} = 20^\circ$, $a = 0$; (c) $\theta_{\text{obs}} = 80^\circ$, $a = 1$; (d) $\theta_{\text{obs}} = 20^\circ$, $a = 1$. Results from this figure are summarized in Tab. 1.

Hardcopy of figures are available upon request from the authors. You can also retrieve the complete postscript file of this paper.

Figure 1: V. Karas & P. Kraus

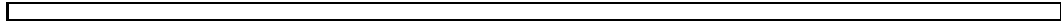


Figure 2: V. Karas & P. Kraus

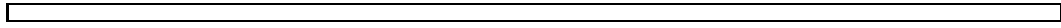


Figure 3: V. Karas & P. Kraus

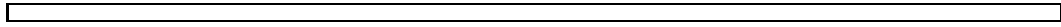


Table 1. Characteristics of the centroid frequency

θ_{obs} [deg]	r_{em}/r_g	$a = 0$				$a = 1$			
		$\nu_{\text{c,max}}$	$\nu_{\text{c,min}}$	$\Delta\nu_{\text{c}}$	$\bar{\nu}$	$\nu_{\text{c,max}}$	$\nu_{\text{c,min}}$	$\Delta\nu_{\text{c}}$	$\bar{\nu}$
80	3	1.32	0.53	1.52	1.13	1.31	0.51	1.55	1.19
20	3	0.84	0.60	0.39	0.83	0.68	0.52	0.29	0.67
80	5	1.26	0.62	1.05	1.00	1.31	0.51	1.55	1.08
20	5	0.95	0.74	0.28	0.95	0.83	0.59	0.41	0.83
80	8	1.23	0.71	0.74	0.99	1.27	0.58	1.20	0.93
20	8	0.98	0.82	0.18	0.98	0.92	0.71	0.28	0.92